

**Integrated Block and Coupling Models of Northern California Faults
from GPS, InSAR and Seismicity: Collaborative Research with Univer-
sity of California, Berkeley and Harvard University**

Collaborative awards G10AP00071 and G10AP00072

June 1, 2010 – May 31, 2011

Principal Investigators

Roland Bürgmann

389 McCone Hall

Dept. of Earth and Planetary Science

Berkeley Seismological Laboratory

University of California, Berkeley

Berkeley, CA 94720-4767

E-mail: burgmann@seismo.berkeley.edu

Phone/Fax: 510-643-9545/510-643-9980

Brendan Meade

Department of Earth & Planetary Sciences

Harvard University, Cambridge

E-mail: meade@fas.harvard.edu

Phone/Fax: 617-495-8921/617-495-7660

Co-Investigators and Project Participants

Ingrid Johanson, Berkeley Seismological Laboratory

Eileen Evans, Harvard University

Jack Loveless, Harvard University, now at Smith College

Integrated Block and Coupling Models of Northern California Faults from GPS, InSAR and Seismicity: Collaborative Research with University of California, Berkeley and Harvard University

Abstract

Space geodetic data provide valuable information about fault slip rates and seismic potential of major faults in the San Francisco Bay area. The most recent update of the Bay Area Global Positioning System (GPS) velocity field (Version 3.0 β) includes campaign and continuous data from 1992-2010. Data collected by InSAR satellites since 1992 form a valuable complement to the GPS measurements. Interferograms provide denser coverage than is possible with GPS. Precise and comprehensive measurements of crustal deformation using GPS and InSAR across the region are used to estimate active fault slip rates and to evaluate the distribution of seismic and aseismic slip on the Concord and Hayward faults. Detailed analysis of InSAR data document 2-5 mm/yr creep rates along the Concord fault, comparable to the long-term slip rate estimates of this fault. To better constrain the kinematic parameters necessary for quantitative seismic hazard assessment, we invert GPS and InSAR data with a kinematically consistent block model of the Bay Area fault system to estimate fault slip rates and spatially variable slip deficit rates on the Hayward fault. Checkerboard resolution tests on the Hayward fault reveal that slip deficit features <15 km long are well resolved along strike at the surface, but cannot be robustly re-solved deeper than 7 km with the current data. We identify a strongly coupled asperity with a slip deficit rate of 3.7 ± 1.2 mm/yr at the surface near San Leandro, CA. Spatial correlation between high slip deficit rates and gabbroic fault surfaces adjacent to the mapped surface trace of the 1868 $MW = 6.9-7.0$ suggest that fault behavior may be associated with complex lithologically modulated variations in frictional behavior.

Integrated Block and Coupling Models of Northern California Faults from GPS, InSAR and Seismicity: Collaborative Research with University of California, Berkeley and Harvard University

Geodetic Monitoring of Active Bay Area Deformation

Imaging strain accumulation about faults with sufficient precision and spatio-temporal resolution is a difficult task, plagued especially by limits in the accuracy and spatial density of the surface measurements. A mix of campaign mode (SGPS) yearly GPS measurements and data from a core network of continuously operating GPS stations (CGPS) of the BARD and PBO networks contribute to a precise (at mm/yr level) representation of the surface velocity field. This project incorporates processing, analysis and integration of a comprehensive GPS data set for central California, building on the BAVU velocity field (Figure 1). The sparsely distributed, but continuously operating CGPS BARD and PBO networks provide a precise 3D geodetic framework with high temporal resolution. Repeated campaign GPS measurements in the Bay Area by our group and data obtained by the USGS provide appropriate densification of precise regional surface velocities to determine long-term strain accumulation rates.

The BAVU velocity field (Version 3.0 β in Figure 1) forms a core component of the recently developed California-wide velocity map (CMM 4), developed by D. Agnew, R. King, Z-K Shen, and M. Murray. This velocity model, provided to the California Earthquake Authority (CEA), includes data from the SCEC Crustal Motion Map (CMM 3) (1986-2001), the SCIGN CGPS network (1996-2003), BAVU (1993-2003), and northern California and Pacific Northwest SGPS networks (1993-2004). We believe it is important to continually update and improve the BAVU time series and velocity solutions for use by the research community, and include future versions of the crustal motion map. Here we present a preliminary version of the most recent BAVU update (Version 3.0 β) that includes campaign and continuous data from 1992-2010.

Data collected by InSAR satellites since 1992 form a valuable complement to GPS measurements. Interferograms provide denser coverage than would be possible with GPS and the data can be acquired at monthly intervals (Figure 2). Standard InSAR measurements are often hampered by significant noise introduced by atmospheric delays and by loss of coherence in vegetated or high-relief terrain. An advanced InSAR processing technique, the Permanent Scatterer method (PS-InSAR; e.g., *Ferretti et al.*, 2004), allows for the identification of individual phase-stable points (outcrops, buildings, utility poles, etc.) in all SAR images of an area of interest. This approach is particularly well suited for use with images over urban areas, where man-made structures make for radar-bright and phase-stable reflectors, but also including sufficient data points in some more remote areas. The PS-InSAR method can measure surface motions at < 1 mm/yr and can resolve very small-scale features not previously recognized by GPS measurements or conventional SAR interferometry over the Bay Area (e.g., *Ferretti et al.*, 2004; *Hilley et al.*, 2004; *Bürgmann et al.*, 2006).

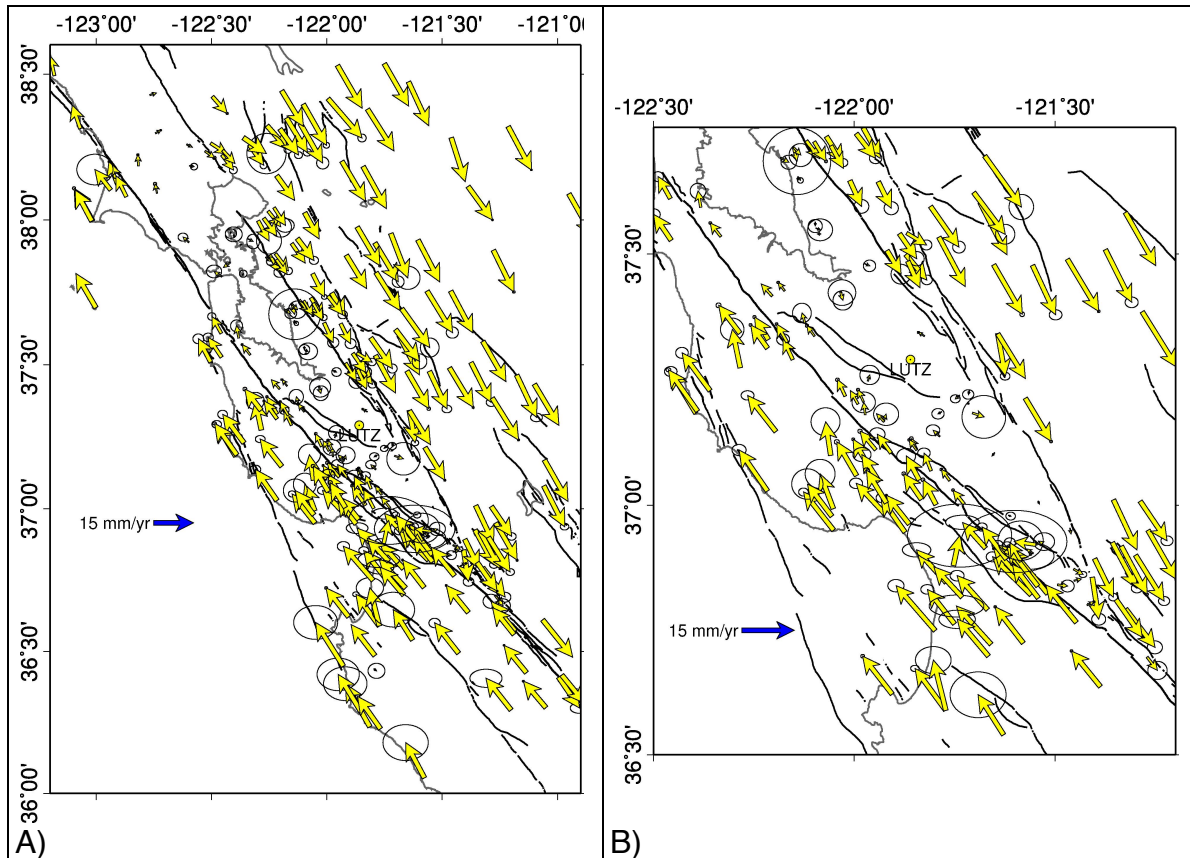


Figure 1. (A) The BAVU 3.0 β velocity field (preliminary) referenced to local site (LUTZ) on the central Bay Block spanning 1992-2010. (B) Detail of complex deformation in the Southern Bay Area, at the junctions of the San Andreas, Calaveras and Hayward faults.

BAVU – Bay Area Velocity Unification

Our GPS analysis relies on the GAMIT/GLOBK processing and analysis system developed at the Massachusetts Institute of Technology (*King et al., 2005; Herring et al., 2005*). We combine daily ambiguity-fixed, loosely constrained solutions using the Kalman filter approach implemented by GLOBK (*Herring et al., 2005*). For Version 3.0 β , we include data processed locally as well as solutions for the IGS, PBO and BARD networks processed by SOPAC at the Scripps Institution of Oceanography (<http://sopac.ucsd.edu/>). Using the Kalman filter, we combine all daily solutions to generate an average solution for each month, giving each observation equal weight. The final positions and velocities are fixed to the ITRF2005 global reference frame (*Altamimi et al., 2007*). Average linear velocities for each station are estimated from the monthly files. Example time series from BAVU 3.0 β are shown in Figure 3, illustrating the scatter in monthly combinations for both the campaign and continuous stations and the long time span of the data that is the backbone of BAVU. One benefit of this data analysis approach lies in the increased ease in which the processing can be integrated with data products from the regional BARD and PBO GPS sites and the global IGS network, which significantly improves the reference stability and also the precision of our velocities. We continue to streamline and automate the BAVU processing scripts, which cover all the steps from data download to production and posting of time series and velocity tables and maps.

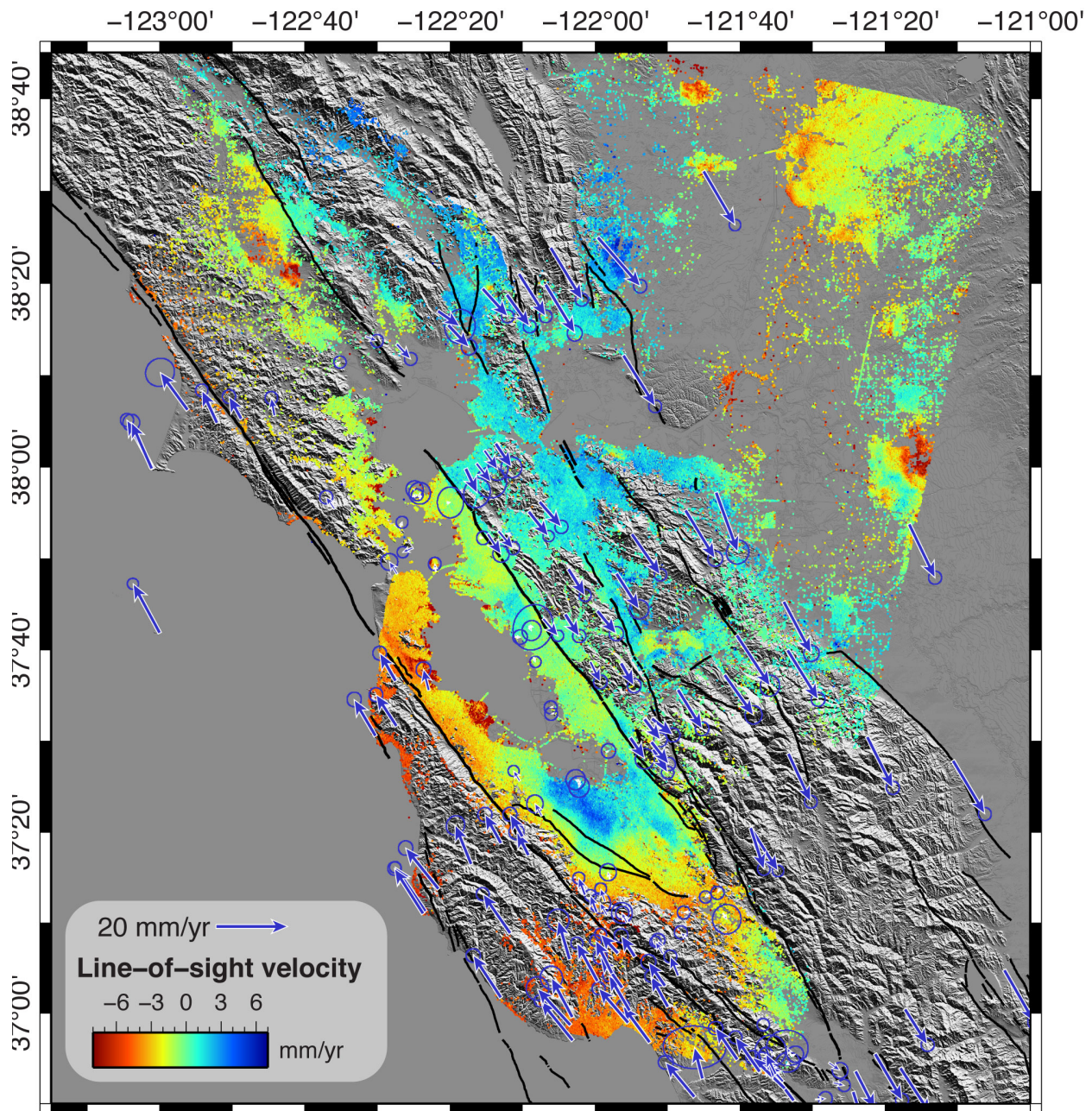


Figure 2. Mosaic of Line-of-sight velocities from PS-InSAR from 1994-2000, calculated using data from the ERS1&2 satellites. Also plotted are GPS velocities from BAVU 2.0.

In official BAVU releases, the errors are scaled following the method used by the Southern California Earthquake Center's Crustal Motion Map team (SCEC CMM 3.0). White noise is added to the formal uncertainties of all stations with a magnitude of 2 mm/yr for the horizontal components and 5 mm/yr for the vertical component. Additionally, 1 mm yr^{-1/2} of Markov process noise is added to account for “benchmark wobble. For Version 3.0 β an abbreviated process is used, and the uncertainties shown in Figure 1 are 1 σ uncertainties in the line fits to the station time series. For Figure 1 a local reference frame is used, centered around station LUTZ (a BARD CGPS site on the Bay Block).

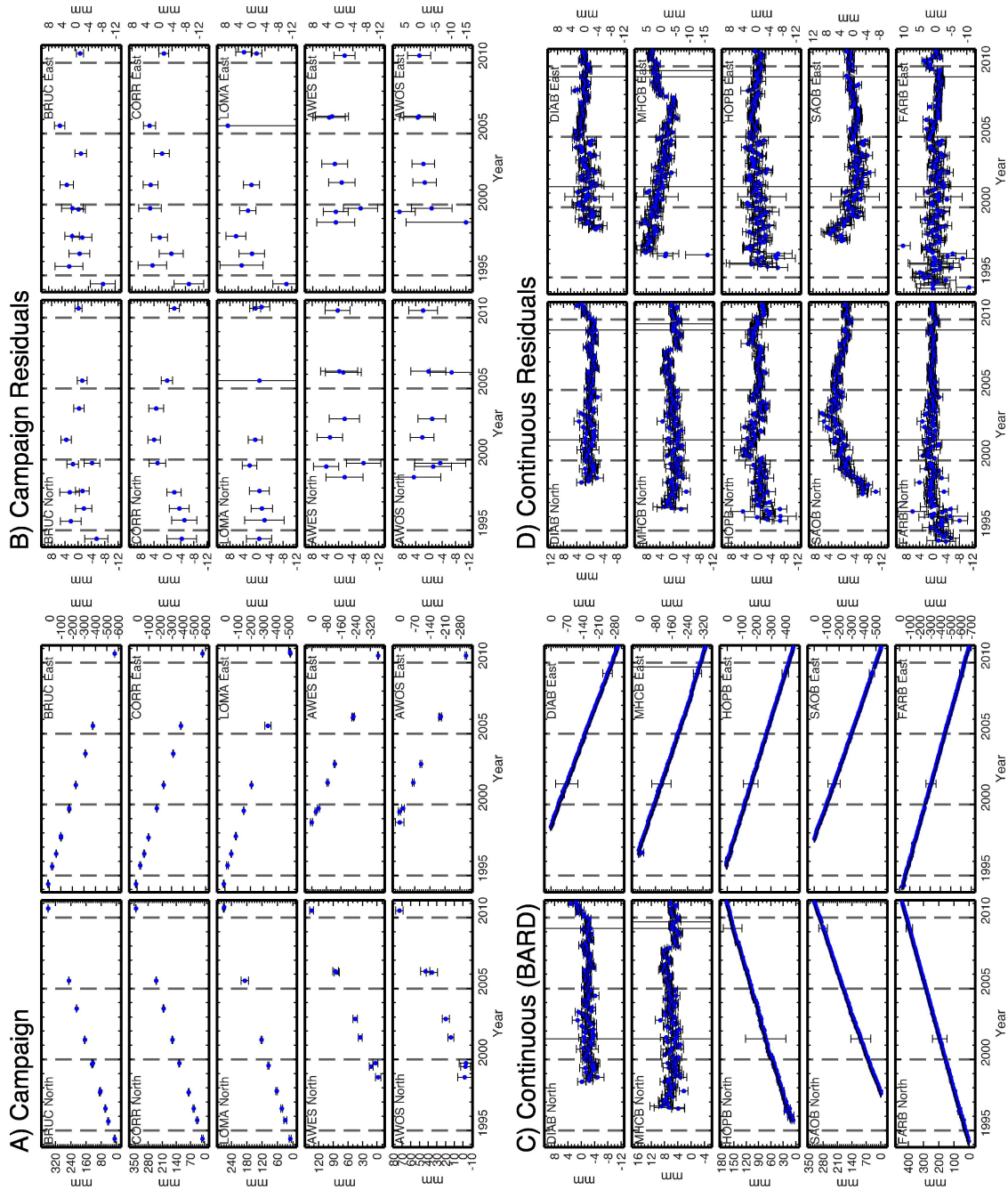


Figure 3. Example time series for campaign (A & B) and continuous (C & D) stations that are part of BAVU 3.0 β . A & C include the linear rate, while C & D are the residuals when the linear rate is removed. Note that here the stations are in the ITRF2005 reference frame, whereas Figure 1 has been re-referenced to station LUTZ. An offset due to the 10/30/2007 Alum Rock earthquake is visible in MHCB, BAVU 3.0 will account for the contribution of earthquakes before estimating the station velocities.

The most significant difference between BAVU 3.0 β and previous versions is the inclusion of many more PBO stations. Over 100 continuous PBO sites have been installed in the Bay Area since the release of BAVU 1.0, beginning in 2006. Most of these new sites now have at least three years of data available and provide robust velocity estimates. Additionally, campaign data

collected last year under a previous NEHRP award has allowed us to leverage data collected in 1996 and 1997 and provide denser coverage in the southern peninsula region of the San Andreas fault (Figure 1B).

East Bay Area Faults – Creep on the Concord Fault

There is some uncertainty in the amount of hazard that the Concord fault represents because of uncertainties both in its long-term slip rate and secular creep rate. Trenching of the Concord fault near Galindo Creek by *Borchardt et al.* (1999) was permissive of slip rates from 3.4-5.4 mm/yr, where 3.4 ± 0.3 mm/yr was the best constrained number and 5.4 mm/yr was the maximum limit. These rates are all slower than the 6.8 ± 1.4 mm/yr determined geodetically from data spanning from 1995-2005 (*d'Alessio et al.*, 2005). The lower geologic rate is similar to the secular creep rates of 2.9-3.7 mm/yr as measured by alignment arrays (AAs) in the central Concord fault (*McFarland et al.*, 2009; *Lienkaemper et al.*, 2011). This would suggest that creep is accommodating nearly all motion on the fault and that large earthquakes will not be generated. However if the current strain accumulation rate is more similar to the geodetic rate, then only half of the Concord fault's slip budget can be accounted for by creep.

At the heart of this discrepancy is the question of to what extent the Concord fault receives slip transferred from the Calaveras and Greenville faults. *d'Alessio et al.*'s block modeling requires connections from both structures to the Concord fault and thus Concord fault slip is a combination of that transferred from the Northern Calaveras and from the Greenville. A long-term slip-rate of 3-4 mm/yr would require only a connection with the Greenville fault.

Both Permanent Scatterers (*Ferretti and Prati*, 2001) and SBAS analysis (*Berardino et al.*, 2002) are time series methods for InSAR data. Time series InSAR has been used successfully in the SFBA to detect and model time dependent motion on landslides in the Berkeley Hills and creep on the Concord and Hayward faults (*Colesanti et al.*, 2003; *Hilley et al.*, 2004; *Lanari et al.*, 2007). We use data from the ERS and Envisat satellites' descending tracks 70 and 342 and ascending track 478. The descending tracks were analysed using the Permanent Scatterers method by Tele-rivimento Europa, while the T478 data was processed using SBAS analysis (Figure 4). The data sets are combined at a high enough level that the difference in initial time series methods shouldn't fundamentally affect the results.

We divide the Concord fault into five profiles, each oriented perpendicular to the local fault strike, for a total of $5 \cdot N$ profiles, where N is the number of SAR scenes in each time series (Figure 4A). The $5N$ profiles are each fit by a simple model consisting of an offset at the fault trace (x_f) and straight line segments on either side.

$$D(x) = C_1 + m_1x + [C_2 + m_2x]H(x - x_f) \quad \text{Equation 1}$$

Where $H(x_f)$ is the Heaviside step function at the fault trace. We fit the model to each profile using the program *est_noise*, which simultaneously fits the model to the data and estimates noise model parameters (*Langbein*, 2004); in this work, we apply a white noise model only.

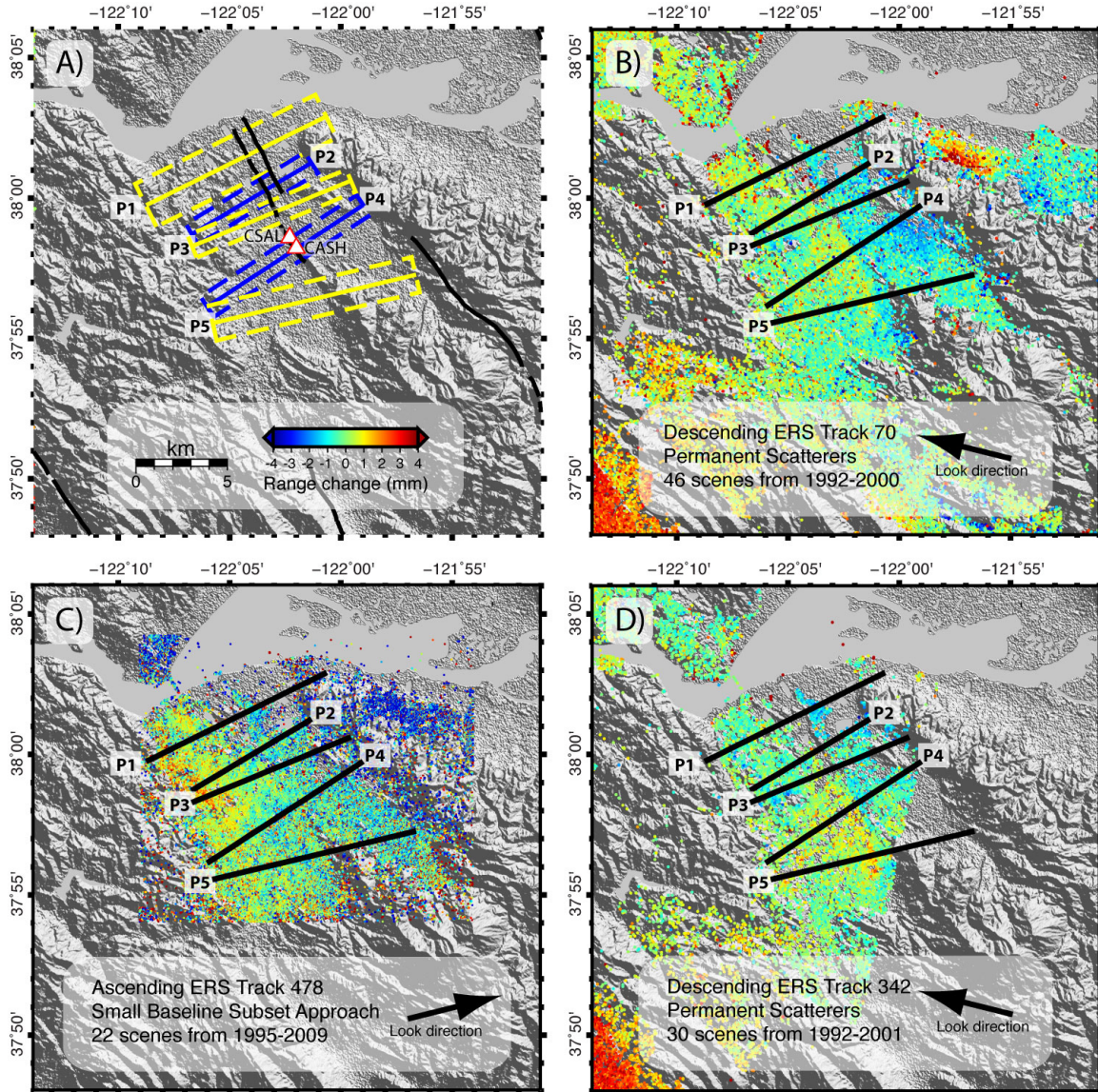


Figure 4. Average velocities from PS-InSAR and SBAS datasets used in this project. A) Location and extent of swaths used for the five profiles, also shown are the locations of two alignment arrays on the Concord fault. Length and color scale in 1A are applicable to all subfigures. B) PS-InSAR, Track 70 C) SBAS, Track 478 D) PS-InSAR, Track 342.

From this, we construct a time series of range change due to fault creep (C_2 in Equation 1) for each profile and again use *est_noise* to determine both a steady rate and a steady rate plus annual sinusoid. While InSAR range change measurements are one dimensional, 3D ground motions can be determined by combining observations from three satellite geometries (*Wright et al.*, 2004). Three geometries are available for the Concord fault because it is covered by two descending orbit tracks: T70 and T342. However, two of them are very similar, such that the three directions of motion are not well resolved. To better constrain the estimate, we assume that all horizontal motion occurs parallel to the Concord fault. This means that only vertical motions and right-lateral strike-slip parallel motions are estimated.

Profile	LOS rates from linear models			LOS rates from linear + sinusoid models		
	Strike-Slip (mm/yr)	Vertical (mm/yr)	RSS	Strike-Slip (mm/yr)	Vertical (mm/yr)	RSS
1	4.2 ± 0.9	0.8 ± 0.2	0.025	3.8 ± 0.9	0.9 ± 0.2	0.023
2	3.8 ± 0.7	0.0 ± 0.2	0.067	3.6 ± 0.6	0.0 ± 0.2	0.053
3	2.3 ± 0.5	0.1 ± 0.1	0.0004	2.5 ± 0.5	0.1 ± 0.1	0.001
4	2.8 ± 0.3	0.4 ± 0.1	0.0006	2.7 ± 0.3	0.4 ± 0.1	0.0001
5	5.3 ± 1.2	-0.3 ± 0.2	0.007	4.4 ± 1.2	-0.1 ± 0.2	0.012

Table 1. Line-of-sight rate determined for each satellite geometry at each profile. Both a straight linear rate and a rate including and annual sinusoid were calculated.

In general the individual profiles are well fit by the block model of Equation 1. Profiles 2 and 4 both show clear and progressively larger offsets on the descending tracks. The offsets on tracks 342 and 478 are not as clear, but nonetheless the modeled offsets on the profiles provide steadily increasing creep estimates. The ascending tracks do not show a sharp offset at the fault trace in any profile and show very little progression of the offsets in the profile models.

The difference between steady rates determined for each profile from models with and without annual sinusoid terms tends to be small. On most profiles, the effect of including an annual term is a modest decrease in the strike-slip creep rate and negligible change to the vertical rates. Profile 5 is the exception; it shows a decrease in creep of nearly 20%, from 5.3 mm/yr to 4.4 mm/yr when an annual sinusoid is included.

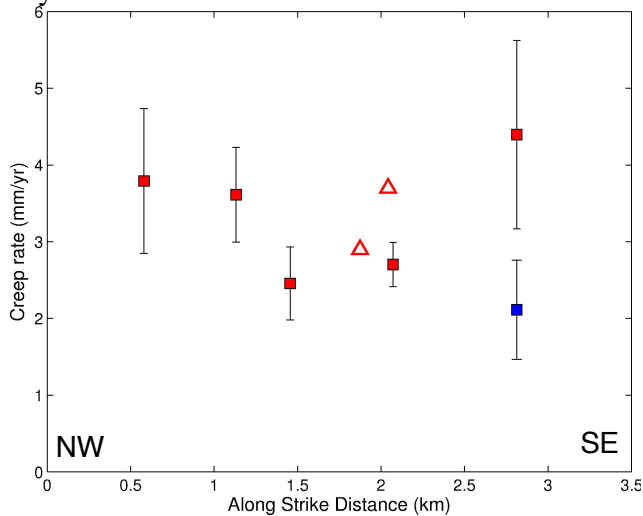


Figure 5. Creep rates on the Concord fault. Along-strike distance is relative to the northern tip of the fault, where it enters the San Joaquin Delta. Two points are plotted for Profile 5: red is determined using the local strike, blue is assuming motion parallel to the regional fault strike. Triangles are the creep rates measured at two alignment arrays.

For both scenarios, creep rates start between 3-4 mm/yr in the north and decrease to 2-3 mm/yr in the central portion of the Concord fault and then increase again at the southern end of the fault (Table 1). The rates determined here match well with alignment array rates for site CASH (3.7 mm/yr) and CSAL (2.9 mm/yr), which both fall within Profile 4 (*McFarland et al.*, 2009). The overall rates of 2-4 mm/yr also match well with estimates from the Galindo Creek trenching of *Borchardt et al.* (1999), which is also located within Profile 4. *Borchardt et al.* found a long-term strike-slip rate of at least 3.4 mm/yr. While the rates estimated here are shallow creep rates, this correspondence means that higher deep slip is not required by our results.

Borchardt et al. (1999) also found a substantial vertical component of fault slip, that averaged to 0.45 ± 0.06 mm/yr. This is similar to the vertical rates determined for Profile 4, but higher than most of the other profiles. Profile 1 has the highest amount of vertical slip, with 0.9 ± 0.2 mm/yr. While the similarity is reassuring, it's important to remember that InSAR tracks the motion of the ground surface, including the effects of groundwater, erosion and deposition, while

the geologic estimate is not affected by these. There are therefore more sources of vertical “noise” that could affect our results.

The time series of range change also reveal variations in fault creep through time. In particular Profiles 3 & 5 for Track 70 show a decrease in creep rate beginning sometime in 1996-1997. Once again, we use *est_noise* and additionally solve for a change in rate beginning on 1/1/1997. The fits to Profiles 3 & 5 are improved by 36% and 34%, respectively while the rest of the profiles have negligible improvement. Profiles 1 & 2, however, are better fit when a step in late 1992 is included (by 40% and 23% respectively, black lines in Figure 6).

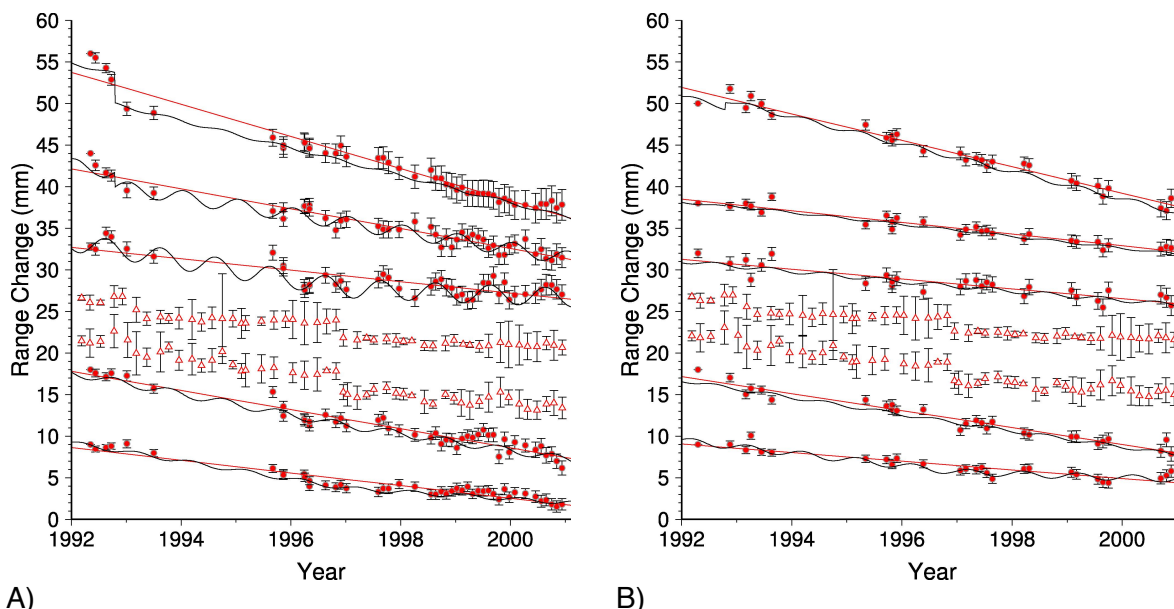


Figure 6. Time series of fault cross-fault line-of-sight values from A) Track 70 and B) Track 342. Both are descending tracks. Uppermost time series are for Profile 1 and lowest are for Profile 5. Triangular data points are from two alignment arrays. Time series are offset vertically for clarity. Red lines show linear fits, while black lines are more complex fits as described in the text.

The InSAR data we use samples farther away from the fault than the alignment arrays and thus averages creep deeper in the fault. Nonetheless, we find creep rates that are very similar to the alignment array results. This indicates that these rates persist to at least ~4km depth (the typical aperture of our profiles). Beyond this it is difficult to determine from the InSAR data whether additional strain accumulation is occurring. Groundwater induced vertical motions in the basin surrounding the Concord fault act to mask the subtle strain accumulation signal. Indeed, the asymmetry of the individual profiles is an indication of how effective it is as a groundwater barrier.

The strike-slip creep rate is highest at the very southern end of the Concord fault (Profile 5). However, this depends strongly on the assumed direction of motion. The InSAR data suggest that the surface trace of the Concord fault bends to the west at its southern end, resulting in a local fault strike that is quite different from the rest of the fault and the highest resulting creep rate. However another interpretation is that there is a righthand step-over between profiles 4 and 5, with the direction of ground motion still parallel to the regional strike. The step-over scenario leads to a creep rate at Profile 5 that is more similar to those for Profiles 2-4 than the fault bend scenario (blue square in Figure 5, Table 2).

Profile	Local Strike	Strike-Slip (mm/yr)	Vertical (mm/yr)	RSS	Regional Fault Strike	Strike-Slip (mm/yr)	Vertical (mm/yr)	RSS
1	-26.3	3.8 ± 0.9	0.9 ± 0.2	0.023	-28	3.6 ± 0.9	1.0 ± 0.2	0.024
2	-31.0	3.6 ± 0.6	0.0 ± 0.2	0.054	-28	4.0 ± 0.7	0.0 ± 0.2	0.052
3	-22.5	2.5 ± 0.5	0.1 ± 0.1	0.001	-28	2.0 ± 0.4	0.2 ± 0.1	0.001
4	-33.2	2.7 ± 0.3	0.4 ± 0.1	0.0001	-28	3.2 ± 0.3	0.3 ± 0.1	0.00002
5	-13.4	4.4 ± 1.2	-0.1 ± 0.2	0.012	-28	2.1 ± 0.6	0.1 ± 0.2	0.017

Table 2. Solutions for strike-slip fault creep and vertical displacement, for motion assumed parallel to the local strike of the fault and those parallel to the regional strike.

A key feature of the alignment array records is the occurrence of creep events every 3-5 years (*McFarland et al., 2009*), such as in late 1996 (Figure 4). No similar offsets are visible from the InSAR data, but the timing of the events matches the timing of the rate changes for Profiles 3 & 5, described above. For both of these profiles, the range change rate decreased after 1997. The InSAR data sample farther away from the fault than the alignment arrays and thus average slip from deeper in the fault. The rate change may reflect a deep transient increase in creep that ended in 1997 and had a longer time signature than the surface creep event. The length of this period of higher creep rates is unclear. If it is the deeper expression of the surface events, then it should occur only at the tail end of the “inter-creep event” period. The data gap from 1994 to almost 1996 makes it difficult to be confident in the pre-1997 rates. Smoothing in the PS and SBAS time series can make it appear that pre-1994 data are part of the period of elevated creep rates, when in fact their offset relative to the rest of the profile may not be so well determined.

Geodetic constraints on San Francisco Bay Area fault slip rates and the partially creeping Hayward fault from block models constrained by GPS and InSAR data

This section of the report is derived from an in review paper entitled “Geodetic constraints on San Francisco Bay Area fault slip rates and potential seismogenic asperities on the partially creeping Hayward fault” by E. L. Evans, J. P. Loveless and B. J. Meade.

Introduction

The Hayward fault is both geometrically [Graymer *et al.*, 2005; Walhauser and Ellsworth, 2000; Hardebeck *et al.*, 2007] and kinematically complex [Lienkaemper *et al.* 2001; Simpson *et al.*, 2001; Schmidt *et al.*, 2005; Funning *et al.*, 2011]. Nearly vertical along most of its trace, the Hayward fault dips eastward south of Fremont, CA, as illuminated by relocated seismicity [Walhauser and Ellsworth, 2002; Manaker *et al.*, 2005; Hardebeck *et al.*, 2007], and likely merges at depth with the Calaveras fault immediately to the east [Ponce *et al.*, 2004; Williams *et al.*, 2005; Graymer *et al.*, 2005]. Surface creep observations from creepmeters [Bilham and Whitehead, 1997] and alignment arrays [Lienkaemper *et al.* 2001; Simpson *et al.*, 2001] show that sections of the Hayward fault creep aseismically with surface creep rates ranging from <4 mm/yr on the northern Hayward fault to 8 mm/yr near Fremont. Estimates of spatially variable creep on the Hayward fault from inversions of GPS and InSAR data [Bürgmann *et al.*, 2000; Schmidt *et al.*, 2005; Funning *et al.*, 2011] suggest that the distribution of interseismic fault coupling is heterogeneous, ranging from 0 to 8 mm/yr over <15 km both along strike and down dip. Dynamically driven models [e.g. Savage and Lisowski, 1995; Simpson *et al.*, 2001, Malservisi *et al.*, 2003] of creep on the Hayward fault have been interpreted to agree favorably with geodetically inferred estimates of creep at depth.

Imaging the interseismic creep on the Hayward fault is complicated because the geodetic observations that provide the greatest resolution of activity at depth [Schmidt *et al.*, 2005] are also influenced by the overlapping interseismic elastic strain fields associated with each of the closely spaced faults of the SFBA fault system [e.g., Freymeuller *et al.*, 1999]. Thus, to some extent, estimates of Hayward fault creep at depth depend on assumptions about the behavior of the rest of the SFBA fault system. Previous geodetically inferred models of Hayward fault behavior can be divided into three classes: 1) those that incorporate spatially dense InSAR measurements near the Hayward fault but do not assume that slip rates are kinematically consistent [Schmidt *et al.*, 2005; Funning *et al.*, 2011], 2) those that assume SFBA fault slip rates are kinematically consistent but do not include spatially dense InSAR measurements near the Hayward fault [Murray and Segall, 2001; Johnson and Fukuda, 2010] and 3) those that both assume SFBA fault slip rates are kinematically consistent and include InSAR measurements [Bürgmann *et al.*, 2000].

We estimate partial creep on the Hayward fault in terms of slip deficit within a kinematically consistent block model of the SFBA fault system, assuming steady state interseismic behavior, similar to previous studies of subduction zone environments [e.g., Wallace *et al.*, 2004; Bürgmann *et al.*, 2005; Loveless and Meade, 2010; McCaffrey, 2009]. In a block model, the upper crust is divided into microplates bounded by faults and fault slip rates are linearly proportional to the differential rotation rates at block boundaries, so that slip rates are kinematically consistent [Matsu'ura *et al.*, 1986; Bennett *et al.* 1996; Souter, 1998; McCaffrey, 2002; Meade and Hager, 2005; Meade and Loveless, 2009]. The particular linear block model formulation

used here [Meade and Loveless, 2009] is similar to that used in other Bay Area studies [Matsu'ura et al., 1986; Murray and Segall, 2001; d'Alessio et al., 2005] with the addition of spatially variable fault coupling on the Hayward fault, and without a priori fault slip rate assumptions [Johnson and Fukuda, 2010].

Geodetic observations and reference block model geometry

Here we modify the block model formulation [Meade and Loveless, 2009] to include InSAR constraints. The geodetic data that we consider are 191 nominally interseismic GPS velocities and 15,000 PS-InSAR (Permanent Scatterer) line-of-sight range change rates collected from 1992 to 2000 by the European Remote Sensing satellites ERS-1 and ERS-2 [Bürgmann et al., 2006]. Survey mode GPS velocities in the SFBA are those reported by d'Alessio et al., [2005], augmented by 6 GPS velocities at sites in the Pacific (sites KWJ1, CHAT, KOKB, MKEA, THTI, MAUI) and 9 in eastern North America (sites WES2, BARN, THU1, THU3, SCH2, BRMU, ALRT, STJO, KELY) to constrain far-field plate motions. Here we are focused on understanding steady interseismic fault system behavior, we do not include velocities from GPS stations that have documented post-seismic deformation following the $M_w = 6.9 - 7.0$ 1989 Loma Prieta Earthquake [Bürgmann et al., 1997]. The InSAR data [Bürgmann et al., 2006] are filtered to remove observations that may be affected by seasonal groundwater effects and local spatially incoherent motions by removing all observations on Quaternary units, and retaining only range change rates of greater than -10 mm/yr and less than 10 mm/yr. We additionally remove observations differing from the mean of all stations within 5 km by more than 1 mm/yr. The resulting filtered InSAR observations were then cropped to remove observations in the Santa Cruz mountains and the Southern Calaveras fault that may be biased by ongoing postseismic deformation from the Loma Prieta Earthquake. The final InSAR data set retains the 15,000 most coherent observations. There are 7,144 observations within 5 km of either side of the Hayward fault, although data density decreases toward the south due to the presence of Quaternary units and vegetation. Within the block model inversion, we account for uncertainties in satellite orbits by simultaneously estimating a best fitting quadratic ramp [e.g., Pritchard et al., 2002, Zebker et al. 1994].

The block geometry for a reference SFBA model is informed by mapped active faults [Graymer et al., 2002] and previous regional crustal deformation studies. We use a reference block model geometry that is similar to d'Alessio et al. [2005]. Our Bay Area plate boundary block model is divided into six blocks making up the deformation zone between the Pacific block to the west and the Sierra Nevada block to the east (Figure 7). The San Francisco peninsula block is separated from the Pacific block by the San Gregorio fault and bounded by the San Andreas fault in the east. East of the San Andreas fault is the Bay block, which is bordered on the east by the Rodgers Creek, Hayward, and Calaveras faults. The East Bay block lies between the Hayward and Rodgers Creek faults to the west and the Northern Calaveras fault to the east. The northeast Bay Area contains the Napa Block, bounded by the West Napa fault in the west and the Green Valley and Concord faults in the east. The Greenville fault separates the East Bay Hills block from the Sierra Nevada block, which bounds the entire SFBA fault system to the east.

The most notable geometric difference between this reference block model and previous models [d'Alessio et al. 2005; Johnson and Fukuda, 2010] is that we do not include the Great Valley fault as a structure sub-parallel to the SAF. Instead, we hypothesize that the Greenville fault in the east Bay Area transfers slip to the Quien Sabe fault. Repeating micro-earthquakes on this structure indicate that it is distinct from the neighboring southern Calaveras fault and may

actively creep [Templeton et al., 2008]. This difference in model geometry is consistent with the idea that all of the slip in the SFBA is fed from San Andreas and San Gregario faults in central California and is discussed in the results section. All faults other than the Hayward fault are represented using rectangular dislocation elements [Okada, 1985] that are assumed to be locked from the surface to an effective locking depth during the interseismic stage of the seismic cycle. InSAR data near the trace of the Hayward fault [Schmidt et al., 2005; Bürgmann et al., 2006; Funning et al., 2011] are spatially dense enough to enable us to constrain spatial variations in fault coupling in this region. Although nearly vertical for most of its trace, the Hayward fault dips east south of Fremont, CA, and likely merges with the Calaveras fault at depth [Waldhauser and Ellsworth, 2002; Manaker et al., 2005; Graymer et al., 2005; Hardebeck et al., 2007]. The geometry of the Hayward fault is represented by the three-dimensional mesh of triangular dislocation elements derived from relocated seismicity and geologic mapping [Murray-Moraleda and Simpson, 2009]. We estimate spatially variable coupling on the portion of the Hayward fault north of the proposed step over to the Calaveras fault east of San Jose. In addition to the reference model described above, we have tested block boundary geometries with and without stepovers on the Calaveras-Concord-Green Valley system and in San Pablo Bay and find negligible differences in slip rate estimates on SFBA faults.

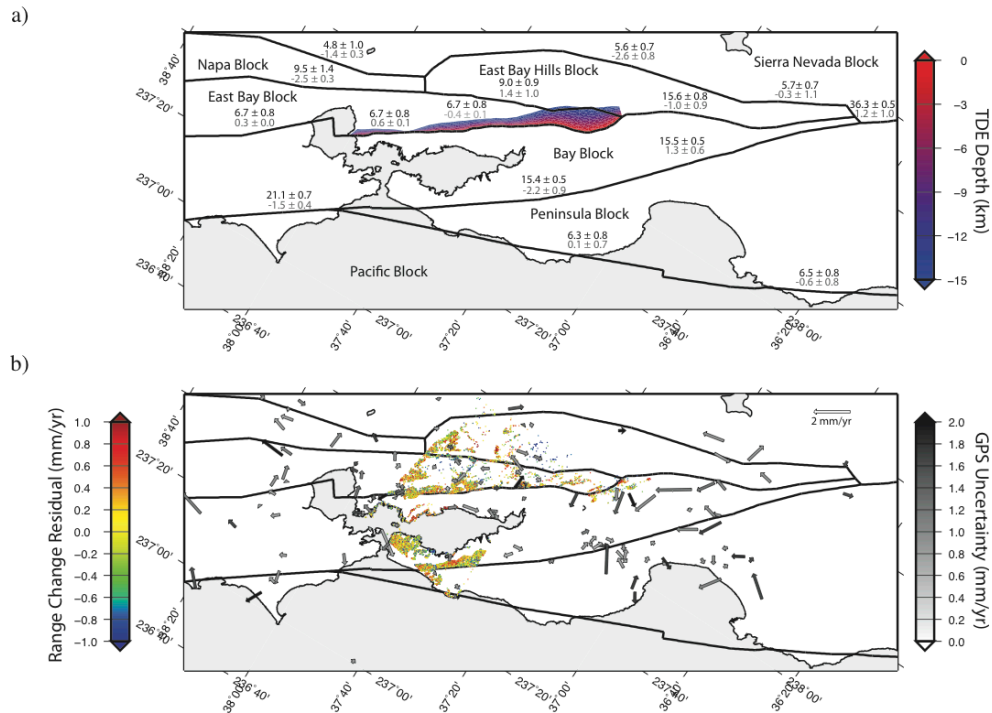


Figure 7. a) Block geometry with labeled blocks. On-fault estimated strike-slip rates are shown in black, dip-slip rates in grey. Negative dip-slip rate is tensile. Mesh of triangular dislocation elements used to estimate spatially variable coupling colored by depth of element. b) Residual InSAR range change rates and GPS velocities

Estimated fault slip and creep rates

Because there are nearly two orders of magnitude more InSAR observations than GPS observations, the InSAR data as a whole have a dominant influence on the solution unless they are downweighted. In our reference model the weighting ratio of the InSAR data relative to the

GPS data, β_{SAR} , is set to 0.1 so that no individual InSAR pixel has more of an influence over the solution than the GPS velocity with the smallest uncertainty. We also regularize the solution by smoothing the slip deficit rates on the mesh of triangular dislocation elements by minimizing the gradient of coupling rate between adjacent triangles [e.g., *Harris and Segall, 1987, Maerten et al., 2005*]. We choose the smoothing constant, β^* , based on the resolution tests described below. In the reference model, $\beta^* = 5$. The reference model reproduces the Bay Area GPS velocity field and InSAR range change rates with a mean residual GPS velocity of 1.4 mm/yr (WRSS per station = 6.1) and mean residual InSAR range change rate of 0.4 mm/yr.

We estimate a slip rate of 9.0 ± 0.9 mm/yr on the Calaveras fault, which is faster than both the previous geologic slip rate estimate of 5.0 ± 2.0 mm/yr [*Simpson et al., 1999*] and the previous geodetic estimate of 6.2 ± 1.0 [*d'Alessio et al., 2005*] (Figure 7). A slip rate estimate of 5.6 ± 0.7 mm/yr on the Greenville fault is consistent with a recent estimates of a minimum geologic fault slip rate of 2 mm/yr from offset sediments [*Berger et al., 2010*]. A slip rate of 5.7 ± 0.7 mm/yr on the Quien Sabe fault is also consistent with estimates of 11 cm of creep offset over 22 years of observations estimated from repeating microearthquakes on the fault [*Templeton et al., 2008*], although the use of repeating microearthquakes as creepmeters is controversial [*Sammis and Rice, 2001*]. We estimate 36.3 ± 0.5 mm/yr on the central San Andreas fault south of Hollister. This is consistent with other geodetic observations in this region [*Johanson and Bürgmann, 2005*], and with estimates north of Parkfield, CA [*Argus and Gordon, 2001; Segall, 2002; Becker et al., 2005, Meade and Hager, 2005; Schmalze et al., 2006*]. This agreement supports the idea that SFBA slip is fed directly from the San Andreas and San Gregario faults in central California.

We estimate that the Hayward fault is fully to partially creeping along its entire length and down to at least 7 km depth (Figure 8). Although short wavelength features (<15 km) cannot be robustly resolved below 7 km depth (see resolution tests below), Figure 8 shows the complete slip deficit and creep rate estimates from the reference model, in which the Hayward fault extends to 15 km depth. Above 7 km, slip deficit rates appear to decrease, and creep rates increase, with depth. We estimate the long-term fault slip rate on the Hayward fault to be 6.7 ± 0.8 mm/yr, which is 1 to 4 mm/yr lower than previous estimates of long-term slip rates on the Hayward fault [*d'Alessio et al., 2005; Lienkaemper and Borchardt, 1996; Graymer et al., 2002*] (Figure 8). Similar to previous Hayward fault studies [e.g., *Simpson et al., 2001; Schmidt et al., 2005; Funning et al., 2011*], we find maximum coupling rates of 4.3 ± 1.4 mm/yr at depth beneath Pt. Pinole, although the lack of InSAR data at the northern end of the fault limits resolution here. High surface creep rates near Pt. Pinole (4.1 ± 2.1 mm/yr) and near Fremont, CA (7.2 ± 1.5 mm/yr) are generally consistent with observations [*Bilham and Whitehead, 1997; Lienkaemper et al., 2001*]. Within 67% confidence bounds, both model surface creep rate estimates and creep rate measurements, agree at 19 of the 25 alignment array observation locations [*Lienkaemper et al., 2001*] (Figure 8a). The southern portion of the creep distribution shows a rapid increase in creep rate at the surface and at depth, supporting the hypothesis that the Hayward fault merges around 90 km from Pt. Pinole with the Calaveras fault to the east [*Waldhauser and Ellsworth, 2002; Galehouse and Lienkaemper, 2003; Ponce et al., 2004; Williams et al., 2005; Manaker et al., 2005; Graymer et al., 2005*]. Between San Leandro and Fremont, spatially coincident with the surface rupture in the 1868 Hayward earthquake [*Lawson, 1908*] and a 25 km long gabbroic body on both faces of the Hayward fault [*Graymer et al., 2005*], we estimate a 20 km long segment with slip deficit rates of up to 3.7 ± 1.2 mm/yr at the surface (Figure 8b).

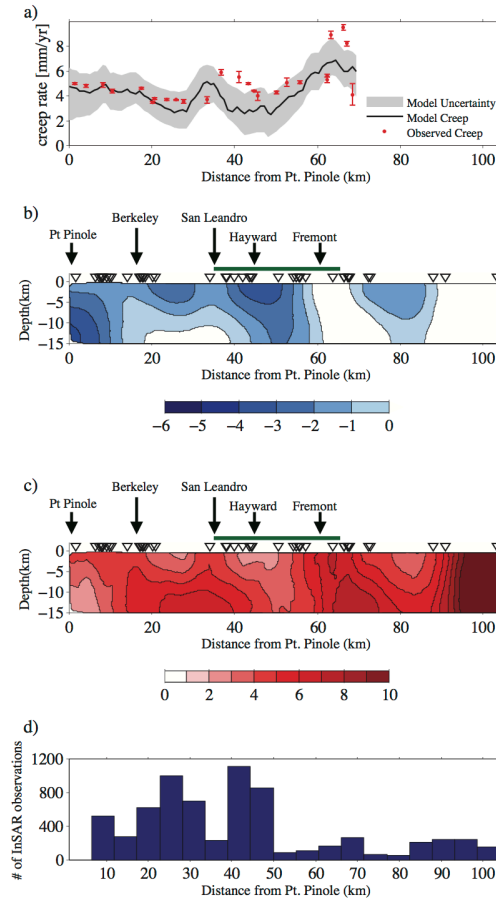


Figure 8. a) Observed creep rates and estimated creep (estimated long term slip - estimated coupling) on the surface triangular dislocation elements of our reference coupling distribution shown with 67% confidence bounds. b) Reference slip deficit distribution on the Hayward fault estimated on a mesh of triangular dislocation elements. High coupling rates (dark blue) correspond to locked regions. Low slip deficit rates (white) represent creeping sections. Black triangles represent GPS station locations. Green bar represents the observed surface trace of the 1868 Hayward earthquake. c) Reference creep distribution (estimated long term slip minus estimated slip deficit rate) for the fault surface. d) Histogram showing density of SAR data points within 5 km of either side of the fault.

Resolution tests

To determine how well the current distribution of GPS and InSAR observations can be used to resolve coupling on the Hayward fault in the context of the elastic block model used here we perform a series of checkerboard resolution tests [e.g., *Bürgmann et al., 2005, Loveless and Meade, 2010*]. We create a synthetic coupling distribution in a checkerboard pattern (Figure 9) in which patches of 20 km by 7.5 km are assigned coupling rates alternating between 10 mm/yr and 0 mm/yr. We run a forward block model (using the same geometry as the reference model) with this known coupling distribution to generate synthetic GPS velocities and synthetic InSAR range change rates at the same observation coordinates as the real data. Inverting the synthetic geodetic data to see how well a known slip deficit distribution can be recovered provides an assessment of the resolving ability of the model at different points along the fault and allows us to objectively

test the sensitivity to variations in weighting parameters. InSAR and GPS data densities within 5 km of the Hayward fault trace are greatest on the northern portion of the fault.

The resolved coupling distribution varies based on the contribution to the solution of InSAR data relative to GPS data and based on the degree of smoothing. When the ratio β_{SAR} is equal to one, every InSAR range change rate is given the same weight as each GPS velocity. Higher β_{SAR} values improve spatial resolution on the triangular dislocation elements due to the greater density of InSAR observations near the fault. Decreasing the smoothing constant β^* for a given data weight ratio sharpens the boundaries between the checkerboards. Figure 9 shows the results of 9 realizations of the checkerboard resolution test with weighting ratio ranging from $\beta_{\text{SAR}} = 0.01$ to $\beta_{\text{SAR}} = 1$ and smoothing values ranging from $\beta^* = 1$ to $\beta^* = 10$. Features at ~ 15 km wavelength are resolvable where $\beta^* = 1$, $\beta_{\text{SAR}} = 1$ (Figure 9). At distances of 40-70 km south of Pt. Pinole, this resolution test overestimates coupling by ~ 1 mm/yr at the surface and underestimates coupling by ~ 2 mm/yr at depth. Farther south than 70 km, resolution at depth deteriorates such that we estimate only 5 mm/yr of the input 10 mm/yr patch at depth between 70 and 90 km from Pt. Pinole (Figure 9).

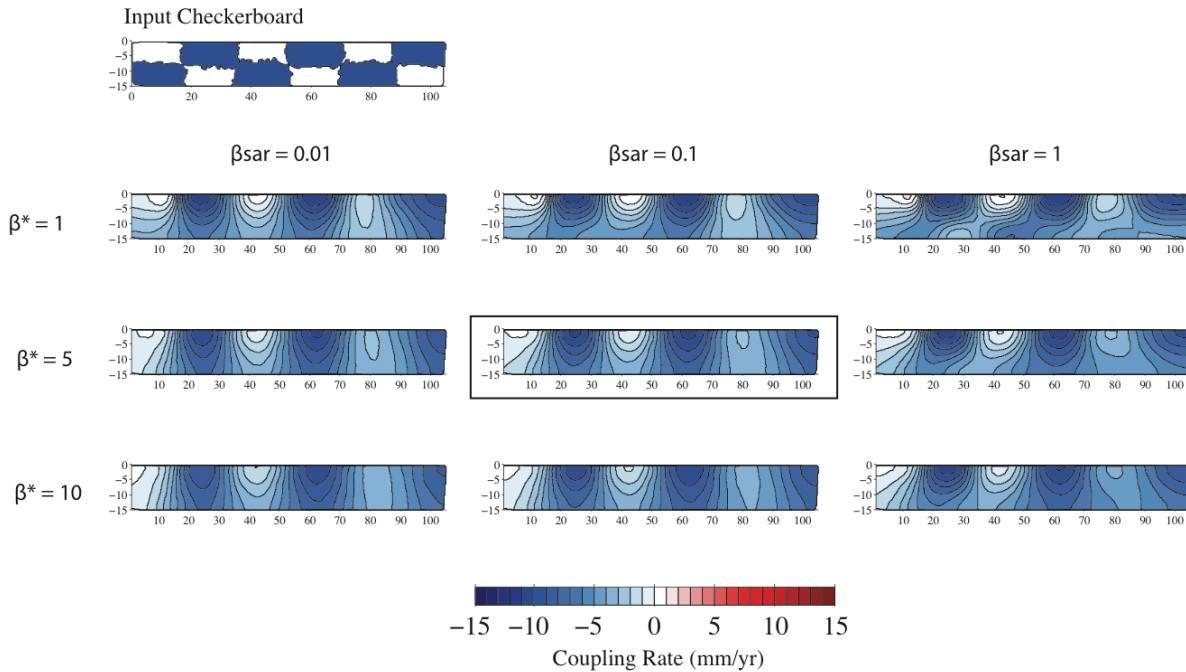


Figure 9. Checkerboard resolution tests without noise. We assign a known coupling distribution (Input Checkerboard) to the Hayward fault mesh of triangular dislocation elements, generate synthetic GPS and InSAR surface observations with a forward model. We then add noise sampled from a normal distribution with mean of 1 mm/yr and invert to recover the input coupling distribution. Contribution to the solution from InSAR relative to GPS, $\beta_{\text{SAR}} = 1$, increases from left to right. The smoothing constant $\beta^* = 1$ increases from top to bottom. Constants corresponding to the reference model shown with black box.

We choose a smoothing value of $\beta^* = 5$ and weight ratio of $\beta_{\text{SAR}} = 0.1$ for our reference model to capture along strike coupling variations with minimal overshoot in the coupling rate estimates. These resolution tests demonstrate that we are able to resolve coupling features of 15-20 km in wavelength along strike, especially between 10 and 80 km from Pt. Pinole. At high smoothing weights, resolution at depth deteriorates. With a InSAR weight, $\beta_{\text{SAR}} = 0.1$, and smoothing weight, $\beta^* = 5$, the checkerboard resolution tests are not successful at recovering slip deficit features <15 km in length below 7 km depth. In interpreting model results, slip deficit estimates deeper than 7 km should be considered within the context of these resolution tests.

Summary

To better constrain the kinematic parameters necessary for quantitative seismic hazard assessment, we invert GPS and InSAR data with a kinematically consistent block model of the SFBA fault system to estimate Bay Area fault slip rates and spatially variable slip deficit rates on the Hayward fault. Checkerboard resolution tests on the Hayward fault reveal that slip deficit features <15 km long are well resolved along strike at the surface, but cannot be robustly resolved deeper than 7 km with the current data. We identify a strongly coupled asperity with a slip deficit rate of 3.7 ± 1.2 mm/yr at the surface near San Leandro, CA. Spatial correlation between high slip deficit rates and gabbroic fault surfaces adjacent to the mapped surface trace of the 1868 $M_w = 6.9-7.0$ suggest that fault behavior may be associated with complex lithologically modulated variations in frictional behavior. Further insight into whether or not geodetically imaged asperities limit the rupture extent of future earthquakes on the Hayward fault may be gained through dynamic slip models that are evolved forward in time from present day conditions.

References

- Altamimi, Z., X. Collilieux, J. Legrand, B. Garayt, and C. Boucher (2007), ITRF2005: A new release of the International Terrestrial Reference Frame based on time series of station positions and Earth Orientation Parameters, *J. Geophys. Res.*, 112, B09401, doi:10.1029/2007JB004949.
- Argus, D. F., and R. G. Gordon (2001), Present tectonic motion across the Coast Ranges and San Andreas fault system in central California, *Geological Society of America Bulletin*, 113(12), 1580-1592.
- Becker, T. W., J. L. Hardebeck, and G. Anderson (2005), Constraints on fault slip rates of the southern California plate boundary from GPS velocity and stress inversions, *Geophysical Journal International*, 160(2), 634-650.
- Bennett, R. A., W. Rodi, and R. E. Reilinger (1996), Global positioning system constraints on fault slip rates in southern California and northern Baja, Mexico, *Journal of Geophysical Research-Solid Earth*, 101(B10), 21943-21960.
- Berardino, P., G. Fornaro, R. Lanari, and E. Sansosti (2002), A new algorithm for surface deformation monitoring based on small baseline differential SAR interferograms, *IEEE Trans. Geosci. Remote Sensing*, 40(11), 2375-2383, doi:10.1109/TGRS.2002.803792.
- Berger, G. W., T. L. Sawyer, and J. R. Unruh (2010), Single- and Multigrain Luminescence Dating of Sediments Related to the Greenville Fault, Eastern San Francisco Bay Area, California, *Bulletin of the Seismological Society of America*, 100(3), 1051-1072.
- Bilham, R., and S. Whitehead (1997), Subsurface creep on the Hayward fault, Fremont, California, *Geophysical Research Letters*, 24(11), 1307-1310.

- Borchardt, G. A., D. L. Snyder, and C. J. Wills (1999), Holocene slip rate of the Concord fault at Galindo Creek in Concord, California, *U.S. Geological Survey National Earthquake Hazards Reduction Program, Final Technical Report*, (1434-HQ-97-GR-03102.) Bürgmann et al., 2006
- Bürgmann, R., P. Segall, M. Lisowski, and J. Svarc (1997), Postseismic strain following the 1989 Loma Prieta earthquake from GPS and leveling measurements, *Journal of Geophysical Research-Solid Earth*, 102(B3), 4933-4955.
- Bürgmann, R., G. Hilley, A. Ferretti, and F. Novali (2006), Resolving vertical tectonics in the San Francisco Bay Area from permanent scatterer InSAR and GPS analysis, *Geology*, 34(3), 221-224.
- Bürgmann, R., M. G. Kogan, G. M. Steblov, G. Hilley, V. E. Levin, and E. Apel (2005), Interseismic coupling and asperity distribution along the Kamchatka subduction zone, *Journal of Geophysical Research-Solid Earth*, 110(B7).
- Bürgmann, R., D. Schmidt, R. M. Nadeau, M. d'Alessio, E. Fielding, D. Manaker, T. V. McEvelly, and M. H. Murray (2000), Earthquake potential along the northern Hayward fault, California, *Science*, 289(5482), 1178-1182.
- Colesanti, C., A. Ferretti, F. Novali, C. Prati, and F. Rocca (2003), Sar monitoring of progressive and seasonal ground deformation using the permanent scatterers technique, *IEEE Trans. Geosci. Remote Sensing*, 41(7), 1685-1701, doi:10.1109/TGRS.2003.813278d'Alessio et al., 2005)
- d'Alessio, M. A., I. A. Johanson, R. Bürgmann, D. A. Schmidt, and M. H. Murray (2005), Slicing up the San Francisco Bay Area: block kinematics and fault slip rates from GPS-derived surface velocities, *Journal of Geophysical Research-Solid Earth*, 110(B6).
- Ferretti, A., and C. Prati (2001), Permanent scatterers in SAR interferometry, *IEEE Trans. Geosci. Remote Sensing*, 39(1), 8-20.
- Ferretti, A., F. Novali, R. Bürgmann, and G. Hilley (2004), InSAR permanent scatterer analysis reveals ups and downs in San Francisco Bay area, *Eos Trans AGU*, 85(34), 317, doi:10.1029/2004EO340002.
- Frey Mueller, J. T., M. H. Murray, P. Segall, and D. Castillo (1999), Kinematics of the Pacific North America plate boundary zone, northern California, *Journal of Geophysical Research-Solid Earth*, 104(B4), 7419-7441.
- Funning, G. J., R. Bürgmann, A. Ferretti, and F. Novali (2011), The source of major earthquakes on the Hayward fault, California, submitted.
- Galehouse, J. S., and J. J. Lienkaemper (2003), Inferences drawn from two decades of alignment array measurements of creep on faults in the San Francisco Bay Region, *Bulletin of the Seismological Society of America*, 93(6), 2415-2433.
- Graymer, R. W., A. M. Sarna-Wojcicki, J. P. Walker, R. J. McLaughlin, and R. J. Fleck (2002), Controls on timing and amount of right-lateral offset on the East Bay fault system, San Francisco Bay region, California, *Geological Society of America Bulletin*, 114(12), 1471-1479.
- Graymer, R. W., D. A. Ponce, R. C. Jachens, R. W. Simpson, G. A. Phelps, and C. M. Wentworth (2005), Three-dimensional geologic map of the Hayward fault, northern California: Correlation of rock units with variations in seismicity, creep rate, and fault dip, *Geology*, 33(6), 521-524.
- Hardebeck, J. L., A. J. Michael, and T. M. Brocher (2007), Seismic velocity structure and seismotectonics of the eastern San Francisco Bay Region, California, *Bulletin of the Seismological Society of America*, 97(3), 826-842.

- Harris, R. A., and P. Segall (1987), Detection of a locked zone at depth on the Parkfield, CA segment of the San Andreas Fault, *Journal of Geophysical Research-Solid Earth and Planets*, 92(B8), 7945-7962.
- Herring, T. A. (2005), GLOBK, Global Kalman filter VLBI and GPS analysis program, Version 10.2, Mass. Instit. of Tech.
- Hilley, G., R. Bürgmann, A. Ferretti, F. Novali, and F. Rocca (2004), Dynamics of slow-moving landslides from permanent scatterer analysis, *Science*, 304(5679), 1952–1955 King *et al.*, 2005
- Johanson, I. A., and R. Bürgmann (2005), Creep and quakes on the northern transition zone of the San Andreas fault from GPS and InSAR data, *Geophysical Research Letters*, 32(14).
- Johnson, K. M., and J. Fukuda (2010), New methods for estimating the spatial distribution of locked asperities and stress-driven interseismic creep on faults with application to the San Francisco Bay Area, California, *Journal of Geophysical Research-Solid Earth*, 115.
- Lawson, A. C. (Ed.) (1908), *The California Earthquake of April 18, 1906*, Report of the State Earthquake Investigation Commission, vol1, Carnegie Inst. of Washington, Washington, D.C.
- Lanari, R., F. Casu, M. Manzo, and P. Lundgren (2007), Application of the SBAS-DInSAR technique to fault creep: A case study of the Hayward fault, California, *Remote Sensing of Environment*, 109(1), 20–28, doi:10.1016/j.rse.2006.12.003.Langbein, 2004
- Lienkaemper, J., F. S. McFarland, R. W. Simpson, R. G. Bilham, D. A. Ponce, and S. J. Caskey (2011), Hayward Fault: Long-term Creep Rates Suggest a Large Locked Patch Controls the Size and Frequency of its Large Earthquakes, *Bull. Seismol. Soc. Am.*, submitted.
- Lienkaemper, J. J., and G. Borchardt (1996), Holocene slip rate of the Hayward fault at Union City, California, *Journal of Geophysical Research-Solid Earth*, 101(B3), 6099-6108.
- Lienkaemper, J. J., J. S. Galehouse, and R. W. Simpson (2001), Long-term monitoring of creep rate along the Hayward fault and evidence for a lasting creep response to 1989 Loma Prieta earthquake, *Geophysical Research Letters*, 28(11), 2265-2268.
- Loveless, J. P., and B. J. Meade (2010), Geodetic imaging of plate motions, slip rates, and partitioning of deformation in Japan, *Journal of Geophysical Research-Solid Earth*, 115.
- Maerten, F., P. Resor, D. Pollard, and L. Maerten (2005), Inverting for slip on three-dimensional fault surfaces using angular dislocations, *Bulletin of the Seismological Society of America*, 95(5), 1654-1665.
- Malservisi, R., C. Gans, and K. P. Furlong (2003), Numerical modeling of strike-slip creeping faults and implications for the Hayward fault, California, *Tectonophysics*, 361(1-2), 121-137.
- Manaker, D. M., A. J. Michael, and R. Bürgmann (2005), Subsurface structure and kinematics of the Calaveras-Hayward fault stepover from three-dimensional V-P and seismicity, San Francisco Bay region, California, *Bulletin of the Seismological Society of America*, 95(2), 446-470.
- Matsu'ura, M., D. D. Jackson, and A. Cheng (1986), Dislocation model for aseismic crustal deformation at Hollister, California, *Journal of Geophysical Research-Solid Earth and Planets*, 91(B12), 2661-2674.
- McCaffrey, R., (2002) Crustal block rotations and plate coupling, in *Plate Boundary Zones*, S. Stein and J. Freymueller, editors, AGU Geodynamics Series 30, 101-122
- McCaffrey, R. (2009), Time-dependent inversion of three-component continuous GPS for steady and transient sources in northern Cascadia, *Geophysical Research Letters*, 36, 5.
- McFarland, F. S., J. J. Lienkaemper, and S. J. Caskey (2009), Data from theodolite measurements of creep rates on San Francisco Bay region faults, California: 1979-2009, *U. S. Geol.*

Survey Open File Rep. 2009-1119

- Meade, B. J., and B. H. Hager (2005), Block models of crustal motion in southern California constrained by GPS measurements, *Journal of Geophysical Research-Solid Earth*, 110(B3).
- Meade, B. J., and J. P. Loveless (2009), Block Modeling with Connected Fault-Network Geometries and a Linear Elastic Coupling Estimator in Spherical Coordinates, *Bulletin of the Seismological Society of America*, 99(6), 3124-3139.
- Murray, M. H., and P. Segall (2001), Modeling broadscale deformation in northern California and Nevada from plate motions and elastic strain accumulation, *Geophysical Research Letters*, 28(22), 4315-4318.
- Murray-Moraleta, J. R., and R. W. Simpson (2009), Geodetically Inferred Coseismic and Post-seismic Slip due to the M 5.4 31 October 2007 Alum Rock Earthquake, *Bulletin of the Seismological Society of America*, 99(5), 2784-2800.
- Okada, Y. (1985), Surface deformation due to shear and tensile faults in a half-space, *Bulletin of the Seismological Society of America*, 75(4), 1135-1154.
- Ponce, D. A., R. W. Simpson, R. W. Graymer, and R. C. Jachens (2004), Gravity, magnetic, and high-precision relocated seismicity profiles suggest a connection between the Hayward and Calaveras Faults, northern California, *Geochemistry Geophysics Geosystems*, 5.
- Pritchard, M. E., M. Simons, P. A. Rosen, S. Hensley, and F. H. Webb (2002), Co-seismic slip from the 1995 July 30 Mw=8.1 Antofagasta, Chile, earthquake as constrained by InSAR and GPS observations, *Geophysical Journal International*, 150(2), 362-376.
- Sammis, C. G., and J. R. Rice (2001), Repeating earthquakes as low-stress-drop events at a border between locked and creeping fault patches, *Bulletin of the Seismological Society of America*, 91(3), 532-537.
- Savage, J. C., and M. Lisowski (1993), Inferred depth of creep on the Hayward fault, central California, *Journal of Geophysical Research-Solid Earth*, 98(B1), 787-793.
- Schmalzle, G., T. Dixon, R. Malservisi, and R. Govers (2006), Strain accumulation across the Carrizo segment of the San Andreas Fault, California: Impact of laterally varying crustal properties, *Journal of Geophysical Research-Solid Earth*, 111(B5).
- Schmidt, D. A., R. Bürgmann, R. M. Nadeau, and M. d'Alessio (2005), Distribution of aseismic slip rate on the Hayward fault inferred from seismic and geodetic data, *Journal of Geophysical Research-Solid Earth*, 110(B8).
- Segall, P. (2002), Integrating geologic and geodetic estimates of slip rate on the San Andreas fault system, *International Geology Review*, 44(1), 62-82.
- Simpson, G. D., J. N. Baldwin, K. I. Kelson, and W. R. Lettis (1999), Late holocene slip rate and earthquake history for the northern Calaveras fault at Welch Creek, eastern San Francisco Bay area, California, *Bulletin of the Seismological Society of America*, 89(5), 1250-1263.
- Simpson, R. W., J. J. Lienkaemper, and J. S. Galehouse (2001), Variations in creep rate along the Hayward Fault, California, interpreted as changes in depth of creep, *Geophysical Research Letters*, 28(11), 2269-2272.
- Souter, B. J. (1998), Comparisons of geologic models to GPS observations in southern California, PhD. Dissertation, Massachusetts Institute of Technology, Cambridge, MA.
- Templeton, D. C., R. M. Nadeau, and R. Bürgmann (2008), Behavior of repeating earthquake sequences in central California and the implications for subsurface fault creep, *Bulletin of the Seismological Society of America*, 98(1), 52-65.
- Waldhauser, F., and W. L. Ellsworth (2000), A double-difference earthquake location algorithm: Method and application to the northern Hayward fault, California, *Bulletin of the Seismol-*

- ological Society of America, 90(6), 1353-1368.
- Waldhauser, F., and W. L. Ellsworth (2002), Fault structure and mechanics of the Hayward Fault, California, from double-difference earthquake locations, *Journal of Geophysical Research-Solid Earth*, 107(B3), 17.
- Wallace, L. M., J. Beavan, R. McCaffrey, and D. Darby (2004), Subduction zone coupling and tectonic block rotations in the North Island, New Zealand, *Journal of Geophysical Research-Solid Earth*, 109(B12).
- Wright, T. J., B. E. Parsons, and Z. Lu (2004), Toward mapping surface deformation in three dimensions using InSAR, *Geophys. Res. Lett.*, 31(L01607), doi:10.1029/2003GL018827.
- Yamanaka, Y., and M. Kikuchi (2004), Asperity map along the subduction zone in northeastern Japan inferred from regional seismic data, *Journal of Geophysical Research-Solid Earth*, 109(B7).
- Yu, E., and P. Segall (1996), Slip in the 1868 Hayward earthquake from the analysis of historical triangulation data, *Journal of Geophysical Research-Solid Earth*, 101(B7), 16101-16118.